Optical spectroscopic study of Eu3+ crystal field sites in Na3La9O3(BO3)8 crystal

C. Cascales, R. Balda, Veronique Jubera, Jean-Pierre Chaminade, J. Fernandez

Optical spectroscopic study of Eu^{3+} crystal field sites in $Na_3La_9O_3(BO_3)_8$ crystal

C. Cascales[1], R. Balda[2], V. Jubera[3], J. P. Chaminade[3], and J. Fernández[2,*]

[1]Instituto de Ciencia de Materiales de Madrid, CSIC, Calle Sor Juana Inés de la Cruz, Cantoblanco, E-28049, Madrid, Spain

[2]Departamento Fisica Aplicada I, Escuela Superior de Ingenieros, Alda. Urquijo s/n 48013 Bilbao, Spain, and Unidad Física de Materiales CSIC-UPV/EHU and Donostia International Physics Center, Apartado 1072, 20080, San Sebastian, Spain

[3]ICMCB CNRS [UPR 9048] - Université Bordeaux 1, 87 av. Dr. A. Schweitzer, 33608 PESSAC cedex France

**Corresponding author: wupferoj@bi.ehu.es*

Abstract: Time-resolved line-narrowed fluorescence spectroscopy of Eu^{3+} ions in a new oxyborate $Na_3La_9O_3(BO_3)_8$ crystal shows the existence of four independent symmetry crystal field sites for the rare-earth ion. A crystal field analysis and simulation of the experimental results have been performed in order to parametrize the crystal field at the Eu^{3+} sites. A plausible argument about the crystallographic nature of these sites is given.

OCIS codes: (140.3380) Laser Materials; (300.6320) Spectroscopy, high resolution.

References and links

1. P. Becker, "Borate materials in Nonlinear Optics," Adv. Mater. **10**, 979-992 (1998).
2. C. Chen, Z. Lin, and Z. Wang, "The development of new borate-based UV nonlinear optical crystals," Appl. Phys. B **80,** 1-25 (2005).
3. B. Braun, F. X. Kartner, U. Keller, J. P. Meyn, and G. Huber, "Passively Q-switched 180-ps Nd:$LaSc_3(BO_3)_4$," Opt. Lett. **21**, 405-407 (1996).
4. D. Jaque, J. Capmany, J. G. Sole, Z. D. Luo, and A. D. Jiang, "Continuous-wave laser properties of the self-frequency-doubling $YAl_3(BO_3)_4$:Nd crystal," J. Opt. Soc. Am. B **15**, 1656-1662 (1998).
5. D. Jaque, J. Capmany, J. A. Sanz Garcia, A. Brenier, G. Boulon, and J. Garcia Sole, "Nd^{3+} ion based self frequency doubling solid-state lasers," Opt. Mater. **13**, 147-157 (1999).
6. D. Jaque, J. Capmany, J. García Solé, "Red, green and blue laser light from a single Nd:$YAl_3(BO_3)_4$ crystal based on laser oscillation at 1.3 μm," Appl. Phys. Lett. **75**, 325-327 (1999).
7. C. Cascales, C. Zaldo, U. Caldiño, J. García Solé, and Z. D. Luo, "Crystal field analysis of Nd^{3+} energy levels in monoclinic $NdAl_3(BO_3)_4$ laser," J. Phys.: Conden. Matter **13**, 8071-8085 (2001).
8. F. Druon, S. Chénais, F. Balembois, P. Georges, A. Brun, A. Courjaud, C. Hönninger, F. Salin, M. Zavelani-Rossi, F. Augé, J. P. Chambaret, A. Aron, F. Mougel, G. Aka, and D. Vivien, "High-power diode-pumped Yb-GdCOB laser: from continuous-wave to femtosecond regime," Opt. Mater. **19,** 73-80 (2002).
9. P. Gravereau, J. P. Chaminade, S Pechev, V. Nikolov, D. Ivanova, and P. Pechev, "$Na_3La_9O_3(BO_3)_8$, a new oxyborate in the ternary system NaO_2-La_2O_3-B_2O_3:preparation and crystal structure," Sol. State Sc. **4,** 993-998 (2002).
10. R. Balda, V. Jubera, C. Frayret, S. Pechev, R. Olazcuaga, P. Gravereau, J. P. Chaminade, M. Al-Saleh, and J. Fernández, "First luminescence study of the new oxyborate $Na_3La_9O_3(BO_3)_8$:Nd^{3+}," Opt. Mater. **30,** 122-125 (2007).
11. C. Cascales, J. Fernández, and R. Balda, "Investigation of site-selective symmetries of Eu^{3+} ions in KPb_2Cl_5 by using optical spectroscopy," Opt. Express **13**, 2141-2152 (2005).
12. C. Cascales, P. Porcher, J. Fernández, A. Oleaga, R. Balda, and E. Dieguéz, "Crystal field studies in Eu^{3+} doped $Bi_{12}SiO_{20}$ and $Bi_{12}SiO_{20}$: V^{5+} crystals," J. Alloys Comp. **323-324,** 260-266 (2001).
13. G. Blasse, A. Bril, and W. C. Nieuwpoort, "On the Eu^{3+} fluorescence in mixed metal oxides. Part I- The crystal structure sensitivity of the intensity ratio of electric and magnetic dipole emission," J. Phys. Chem. Solids **27**, 1587-1592 (1966).
14. C. Görller-Walrand and K. Binnemans, "Rationalization of Crystal-Field Parametrization," in *Handbook on the Physics and Chemistry of Rare Earths*, K. A. Gschneidner Jr. and L. Eyring, eds., (Elsevier Science, Amsterdam, 1996), Vol. 23, pp. 121-283.
15. B. G. Wybourne, *Spectroscopic Properties of Rare Earths*, (Wiley, New York, 1965).
16. C. Cascales M. D. Serrano, F. Esteban-Betegon, C. Zaldo, R. Peters, J. Johannsen, M. Mond, K. Peterman, G. Huber, L. Ackermann, D. Rytz, C. Dupré, M. Rico, U. Griebner, and V. Petrov, "Structural, spectroscopic and tunable laser properties of Yb^{3+}-doped $NaGd(WO_4)_2$," Phys. Rev. B **17**, 174114:1-15 (2006).

#91301 - $15.00 USD Received 3 Jan 2008; revised 7 Feb 2008; accepted 10 Feb 2008; published 12 Feb 2008

17. C. Görller-Walrand, P. Vandevelde, I. Hendrickx, P. Porcher, J-C. Krupa, and G. S. D. King, "Spectroscopic study and crystal field analysis of Eu^{3+} in the $YAl_3(BO_3)_4$ huntite matrix," Inorg. Chim. Acta **143,** 259-270 (1988).

1. Introduction

Since the discovery of laser in the sixties very intense research has been carried out in the field of nonlinear optics aimed to expand the frequency range provided by the known laser materials. New laser sources based on nonlinear optical (NLO) properties of different materials are of common use today, not only in laboratory research but in other fields such as laser diagnosis and therapy, optical telecommunications and signal processing, integrated optics, and many other related fields. Moreover, the development of powerful laser pump diodes has increased the interest to investigate new nonlinear materials for laser applications.

Among NLO materials, the interest in borate compounds has increased in recent years due to their good optical properties such as good transparency in the ultraviolet, high damage threshold, and good nonlinearity which make them promising materials not only for NLO devices [1,2] but also for potential applications in the field of lasers [3-8].

The extraordinary versatility of the borate structure facilitates the design of new compounds. Recently a new oxyborate of formula $Na_3La_9O_3(BO_3)_8$ has been discovered in the ternary Na_2O-La_2O_3-B_2O_3 diagram and its structure resolved [9]. The unit cell is hexagonal with space group P-$\bar{6}$2m (189) and the lanthanum occupies two different crystallographic sites in the structure with coordinations eight and nine. In a very recent work, the authors have presented the first spectroscopic characterization of Nd^{3+} ions in this $Na_3La_9O_3(BO_3)_8$ crystal by using steady-state and time resolved laser spectroscopy [10]. This study shows the existence of at least two different crystal field sites for Nd^{3+} ions in this material in accordance with the existence of two non equivalent crystallographic lanthanum sites. However, a careful examination of the excitation spectra of these ions shows the presence of a complex structure which suggests the existence of other possible crystal field sites for the rare-earth (RE) in this crystal.

It is worthy to mention that the optical properties of rare-earth doped crystals are closely related to local structure and bonding at the ion site. The existence of different crystal field sites may produce spectral broadening and/or multiple emission lines which can influence the energy extraction from the material as well as the wavelength tuning capability when it is used as a lasing medium. As a consequence, the knowledge of the precise crystal field structure of the rare-earth in a given material is of paramount importance to understand its potentialities for lasing applications.

In order to clarify the nature of the RE environments in $Na_3La_9O_3(BO_3)_8$ crystal we have undertaken the study of the site-resolved luminescence of Eu^{3+} in this crystal, taking into account the adequacy of the dopant ion as a structural probe. Since the $^5D_0$ state is nondegenerate under any symmetry, the structure of the $^5D_0 \rightarrow {}^7F_J$ emission is only determined by the splitting of the terminal levels caused by the local crystal field. Moreover, as the $^7F_0$ level is also nondegenerate, site-selective excitation within the inhomogeneous broadened $^7F_0 \rightarrow {}^5D_0$ absorption band can be performed by using the fluorescence line narrowing (FLN) technique to distinguish among different local environments around the rare-earth ions [11,12]. On the ground of the experimental results a crystal-field analysis and simulation of the energy level schemes have also been performed in order to parametrize the crystal-field around the Eu^{3+} ions. As a conclusion, we found evidences about the existence of at least four symmetry independent crystal field sites for the RE ions in this crystal. A plausible argument about the crystallographic nature of these sites is finally given.

2. Experimental techniques

Single crystals were grown by a self flux method, using an excess of the constituents as solvent in the pseudo ternary phase diagram Na_2O-$La_2O_3(Eu_2O_3)$-B_2O_3. Analytical grade purity of Na_2CO_3-$La_2O_3(Eu_2O_3)$-H_3BO_3 reactants with molar ratio 28.51%, 21.52% and

#91301 - $15.00 USD Received 3 Jan 2008; revised 7 Feb 2008; accepted 10 Feb 2008; published 12 Feb 2008

49.95% were weighed (about 100g), ground and mixed, sintered at successively 400°C and 650°C, then melted at 1160°C in a 50 cm^3 Pt crucible in several batches. 0.5 mol% Eu^{3+} doping was chosen.

The growth experiments were carried out in a Kanthal resistance furnace equipped with an Eurotherm controller for temperature and cooling rate regulation. Melting and crystallization temperatures were first determined by using the dipping of a Pt wire. After homogenization of the melt at 1180°C during 24 hours, the temperature was slowly decreased to 1130°C (10°C/h) while the cooling rate was decreased to 0.2°C/h until total solidification took place, and then the furnace was cooled down to room temperature (30°C/h). Crystals grown on the surface of the melt were separated mechanically.

Resonant time-resolved FLN spectra were performed by exciting the sample with a pulsed frequency doubled Nd:YAG pumped tunable dye laser of 9 ns pulsed width and 0.08 cm^{-1} linewidth and detected by an EGG&PAR Optical Multichannel Analyzer. The measurements were carried out by keeping the sample temperature at 10 K in a closed cycle helium cryostat.

For lifetime measurements, the fluorescence was analyzed with a 0.25 m Jobin-Ybon monochromator and the signal detected by a Hamamatsu R636 photomultiplier. Data were processed by a Tektronix oscilloscope.

3. Experimental results

3.1 FLN spectra

Time-resolved line-narrowed fluorescence spectra of the $^5D_0 \rightarrow {}^7F_{0\text{-}6}$ transitions of Eu^{3+} doped $Na_3La_9O_3(BO_3)_8$ crystal were obtained at 10 K by using different resonant excitation wavelengths into the $^7F_0 \rightarrow {}^5D_0$ transition, and at different time delays after the laser pulse. Depending on the excitation wavelength the emission spectra present different characteristics concerning the number of observed $^5D_0 \rightarrow {}^7F_J$ transitions, their relative intensity, and the magnitude of the observed crystal-field splitting for each ^7F_J state. Figure 1 shows the spectra corresponding to the $^5D_0 \rightarrow {}^7F_{0,1,2}$ transitions obtained with a time delay of 10 μs after the pump pulse, at four different pumping wavelengths 581.9, 581.7, 580.4 and 580 nm, which selectively show the presence of four main isolated Eu^{3+} sites.

We shall hereafter refer to the optical features of these spectra as originating from sites A (λ_{exc}= 581.9 nm), B (λ_{exc}= 581.7 nm), C (λ_{exc}= 580.4 nm), and D (λ_{exc}= 580 nm). The presence of the line for the $^5D_0 \rightarrow {}^7F_0$ transition in each spectrum indicates a site of C_{nv}, C_n or C_s symmetry for Eu^{3+}. These symmetries allow the transition as an electric dipole process, according to the group theory selection rules, with a linear term in the crystal-field expansion [13]. The symmetry characteristics of these Eu^{3+} optical centers can be inferred through the comparison among the number of possible and experimentally observed $^5D_0 \rightarrow {}^7F_{0\text{-}6}$ transitions [14], and thus some symmetry point groups can be initially supposed for these Eu^{3+} optical centers.

The spectra obtained with excitation wavelengths 581.9 and 580.0 nm display, in each case, two Stark levels for the $^5D_0 \rightarrow {}^7F_1$ transition and four levels in the hypersensitive $^5D_0 \rightarrow {}^7F_2$ region. These results indicate that Eu^{3+} in A and D sites can be in the presence of a rather higher hexagonal, trigonal or tetragonal symmetry. Given the scarce number of energy levels observed for the $^5D_0 \rightarrow {}^7F_J$ transitions with J>2 we can reasonably extract no more information about specific symmetry point groups from these spectra, a task that must be undertaken under the detailed consideration of the $Na_3La_9O_3(BO_3)_8$ crystal structure, as will be developed in the following Section. On the contrary, the spectrum obtained with the excitation wavelength 581.7 nm shows three Stark levels for the $^5D_0 \rightarrow {}^7F_1$ transition, and five and seven levels for the $^5D_0 \rightarrow {}^7F_2$ and $^5D_0 \rightarrow {}^7F_3$ emissions, respectively, which means that the degeneracy of these three states is completely lifted, that is, the Eu^{3+} B optical center is located in a crystal site with C_{2v} or lower symmetry. Finally, in the spectrum collected with excitation wavelength 580.4 nm, the two and three energy levels for Eu^{3+} site for $^5D_0 \rightarrow {}^7F_1$ and $^5D_0 \rightarrow {}^7F_2$, respectively, indicate a trigonal symmetry for the Eu^{3+} C site, which together with the observation of the $^5D_0 \rightarrow {}^7F_0$ transition, reduces the possibilities to C_{3v} or C_3 point group

#91301 - $15.00 USD Received 3 Jan 2008; revised 7 Feb 2008; accepted 10 Feb 2008; published 12 Feb 2008

symmetries. It is worth noticing that some minor peaks appearing in the spectra of the less intense emissions from sites C and D, probably associated to contributions from Eu^{3+} ions placed in residual/and or interstitial sites have been disregarded.

Table 1 (see Appendix) summarizes the FLN spectral characteristics of A, B, C, and D crystal field sites together with a plausible assignment of crystallographic cationic site for Eu^{3+}. Energy levels observed for transitions from $^5D_0$ to the ground ^7F_J manifold for these main four Eu^{3+} sites are included in Table 2 (see Appendix).

Regarding the relative intensity of the emission coming from the different sites, it is worthy to mention that the highest intensities corresponds to sites A and B, being the intensity from site A around 100 times higher than the one from site B and around three orders of magnitude higher than intensities from sites C and D.

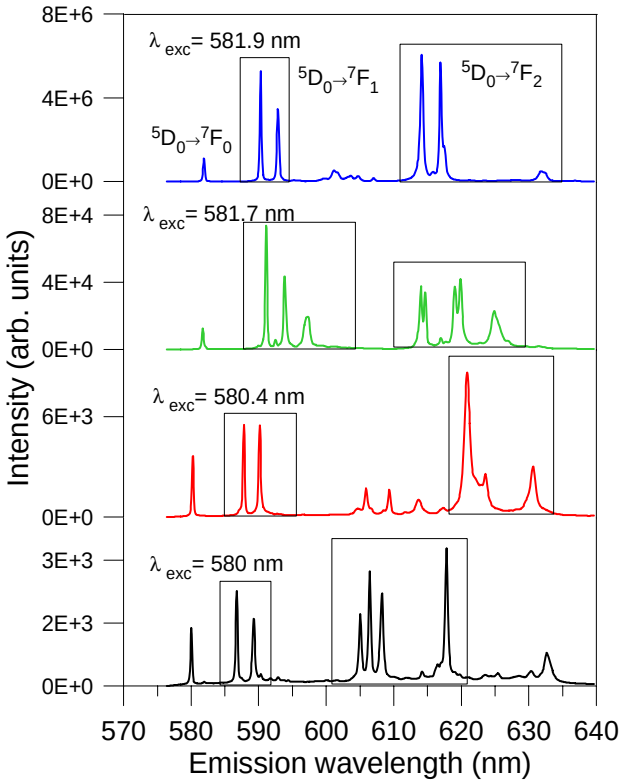

Fig. 1. $^5D_0 \rightarrow {}^7F_{0,1,2}$ emissions of Eu^{3+} in $Na_3La_9O_3(BO_3)_8$ crystal.

3.2 Lifetimes

As could be expected, if there are different sites for the Eu^{3+} ion, the lifetime of state $^5D_0$ should depend on the excitation wavelengths. We have measured the lifetime of the $^5D_0$ state at different excitation wavelengths which correspond to those at which the Eu^{3+} sites are selectively resolved, and collected the luminescence at the highest intensity Stark component of the $^5D_0 \rightarrow {}^7F_2$ transition. The experimental decays are well described by a single exponential function to a good approximation. The values of the measured lifetime are 1.87 ms, 1.73 ms, and 1.32 ms for sites A, B, and C respectively. The low intensity of the emission from site D makes it difficult to measure its lifetime accurately.

#91301 - $15.00 USD Received 3 Jan 2008; revised 7 Feb 2008; accepted 10 Feb 2008; published 12 Feb 2008

4. Crystal-field analysis and simulation of the energy level schemes

The detailed description of the theoretical background of the crystal field analysis and the methods followed to reproduce the experimental sequences of energy levels for Eu^{3+} in A, B, C, and D sites have been previously described [11,12]. In each case, the one-electron crystal field Hamiltonian can be expressed [15] as a sum of products of tensor operators $(C_q^k)_i$, with real B_q^k and complex S_q^k parameters as coefficients, these later appropriated to the Eu^{3+} site symmetry in the host,

$$H_{CF} = \sum_{k=2q=0}^{4,6} \sum^{k} \left[B_q^k (C_q^k + (-1)^q C_{-q}^k) + iS_q^k (C_q^k - (-1)^q C_{-q}^k) \right]$$

detailed as follows:

$$H_{C_{4v}} = B_0^2 C_0^2 + B_0^4 C_0^4 + B_4^4 (C_{-4}^4 + C_4^4) + B_0^6 C_0^6 + B_4^6 (C_{-4}^6 + C_4^6) \quad (1)$$

$$\begin{aligned} H_{C_2} = {} & B_0^2 C_0^2 + B_2^2 (C_{-2}^2 + C_2^2) + S_2^2 (C_{-2}^2 - C_2^2) \\ & + B_0^4 C_0^4 + B_2^4 (C_{-2}^4 + C_2^4) + S_2^4 (C_{-2}^4 - C_2^4) + B_4^4 (C_{-4}^4 + C_2^4) + S_4^4 (C_{-4}^4 - C_2^4) \\ & + B_0^6 C_0^6 + B_2^6 (C_{-2}^6 + C_2^6) + S_2^6 (C_{-2}^6 - C_2^6) + B_4^6 (C_{-4}^6 + C_4^6) + B_4^6 (C_{-4}^6 + C_4^6) + S_6^6 (C_{-6}^6 - C_6^6) \end{aligned} \quad (2)$$

$$H_{C_{3v}} = B_0^2 C_0^2 + B_0^4 C_0^4 + B_3^4 (C_{-3}^4 - C_3^4) + B_0^6 C_0^6 + B_3^6 (C_{-3}^6 - C_3^6) + B_6^6 (C_{-6}^6 + C_6^6) \quad (3)$$

for A and D sites (Eq. 1), B site (Eq. 2) and C site (Eq. 3).

Schemes of 19, 34, 19, and 18 observed Stark levels, included in Table 2, from the total number of 37, 49, 33, and 37, were considered in the simulation of the sequence of Eu^{3+} ^7F_J energy levels in sites A, B, C, and D, with C_{4v}, C_2, C_{3v}, and C_{4v} crystal fields, respectively. Resulting simulated energy levels are also collected in Table 2, and values of their corresponding crystal field parameters and figures of merit of respective fits are included in Table 3 (see Appendix).

5. Correlation of FLN isolated Eu^{3+} sites with the crystal structure

The presence of the above observed Eu^{3+} optical centers must be explained by considering which sites of the $Na_3La_9O_3(BO_3)_8$ crystal structure can accommodate Eu^{3+} cations. Thus, the assignment of each A, B, C or D site to a specific site in the crystal structure must be led by the symmetry-related characteristics of the optical centers resolved in the FLN spectra. Though Eu^{3+} ion usually substitutes lanthanide cations in most of lanthanide-based compounds, in some mixed oxides, containing monovalent cations, these ions may have the same, or nearly the same, oxygen coordination than the one at the lanthanide site giving rise to some structural disorder [16] which facilitates the occupancy of these sites by the RE ions if charge compensation is allowed; therefore, we start this correlation with the inspection of the symmetry characteristics of their oxygen environments.

Following the previous structure description [9], from which the same numbering of atoms has been kept in the subsequent text and in Figs. 2 to 4, $Na_3La_9O_3(BO_3)_8$ crystals present the symmetry of the hexagonal space group $P\bar{6}2m$ (No. 189), with lattice parameters (Å) a = 8.9033(3), c = 8.7131(3), V = 598.14(4), and Z =1; (see Fig. 2). In this oxyborate host La atoms occupy two different crystal sites, 3*g* and 6*i*, coordinated to eight and nine oxygen atoms, respectively. The $La1O_8$ polyhedron can be described as a distorted square antiprism (SAP), with C_{4v} symmetry, and $La2O_9$ is a distorted monocapped square antiprism (MSAP) with C_{2v} (or lower) symmetry; [see Figs. 3(a) and 3(b)]. The Na^+ cations, of only one type, are

#91301 - $15.00 USD Received 3 Jan 2008; revised 7 Feb 2008; accepted 10 Feb 2008; published 12 Feb 2008

surrounded by six oxygen atoms, being the NaO_6 coordination polyhedron described as a highly distorted octahedron; [see Fig. 3(c)]. This coordination is quite unusual for trivalent lanthanides [14], and therefore we have considered an extended oxygen environment which includes oxygen atoms that are not only the nearest neighbors indicated above. Four additional O3, from close $La1O_8$, $La2O_9$ and $B3O_3$ polyhedra, are found at a distance of 3.185(3) Å from Na^+, in such a way that the oxygen distribution of the current NaO_{10} polyhedron can be described as a tetracapped trigonal prism (TTP), with C_{3v} symmetry, which is one of the most frequently observed coordination polyhedra for lanthanide systems; [see Fig. 3(d)].

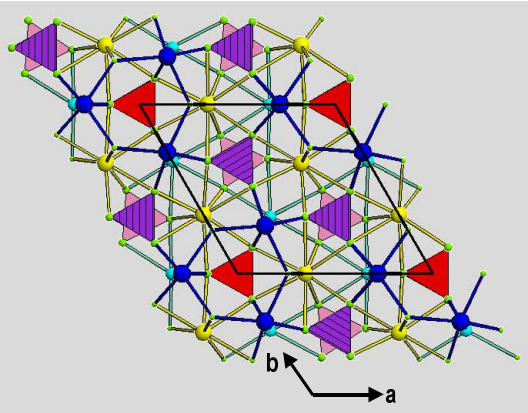

Fig. 2. Projection of the structure of $Na_3La_9O_3(BO_3)_8$ on the *ab* plane. Larger blue and yellow spheres represent La1 and La2 cations, respectively, medium cyan spheres stand for Na cations, red, pink, and violet triangles are indicating $B1O_3$, $B2O_3$ and $B3O_3$ groups, respectively, and the smallest green spheres are the oxygen atoms.

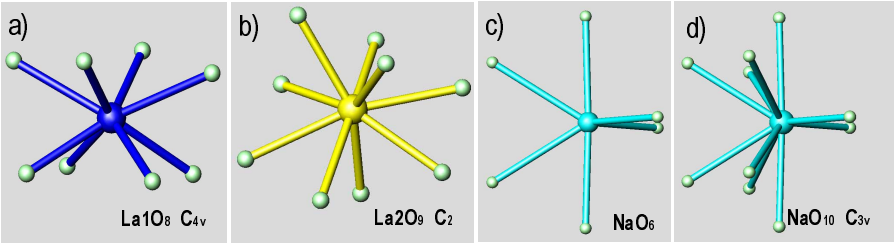

Fig. 3. Coordination polyhedra for cationic sites in the $Na_3La_9O_3(BO_3)_8$ crystal: a) $La1O_8$ C_{4v} distorted square antiprism, b) $La2O_9$ C_2 distorted monocapped square antiprism, c) distorted octahedron NaO_6, and d) extended NaO_{10} C_{3v} tetracapped trigonal prism.

From the above mentioned crystallographic symmetries, the characteristics of which are included in Table 1, it seems reasonable to attribute the spectra of sites A and B to Eu^{3+} located in environments derived from the replacement of La^{3+} in $La1O_8$ and $La2O_9$ polyhedra, respectively. Moreover, the C_{3v} symmetry of the extended NaO_{10} coordination polyhedra could account for the crystal field characteristics found for Eu^{3+} at site C where some kind of additional charge compensation should be expected.

Up to now the La and Na crystal sites can explain the main three among four isolated Eu^{3+} sites in the FLN spectra. Therefore, an additional cationic site possessing the C_{4v} symmetry suggested by the spectroscopic characteristics of the remaining D spectrum, should be identified in the $Na_3La_9O_3(BO_3)_8$ crystal structure.

#91301 - $15.00 USD Received 3 Jan 2008; revised 7 Feb 2008; accepted 10 Feb 2008; published 12 Feb 2008

Returning to the structure description of the $Na_3La_9O_3(BO_3)_8$ crystal [9], it consists of an alternative stacking of layers along the *c*-axis containing Na-$B(2)O(2)_3$ (z = 0), $B(1)O(1)_3$ (z = 0.21), La2 (z = 0.23), $B(3)O(3)_3$ (z = 0.32) and La1O4 (z = 1/2, on the mirror plane); (see Fig. 4). Within this picture, the three $B1O_3$, $B2O_3$ and $B3O_3$ triangles are running in rows along of the *c* axis as shown in Fig. 4. If the sites of boron cations act as *perturbed* Eu^{3+} *sites* induced by the Eu^{3+}-doping itself, they would manifest the C_{4v} symmetry corresponding to the remaining D site in the FLN spectrum. Let us revise the local extended oxygen environments around the three B cations: For Eu^{3+} in the B1 site, three O4 at a distance 3.420(3) Å, and three O1 at 3.917(3) Å, will constitute its extended environment with C_{3v} local symmetry. Correspondingly, Eu^{3+} in the B2 site is surrounded by six O3, all of them at 3.084(3) Å. When the substitution in the B3 site is considered, Eu^{3+} is surrounded by three O2 at 3.145(3) Å, three O3 at 3.419(3) Å, and three O4 at 3.694(3) Å, which could result in a C_{4v} local symmetry. This last perturbed Eu^{3+} site, surrounded by nine oxygen atoms, can be thought of as the origin of the D center, which moreover can be distributed in an ordered way through out the crystal, and thus require nearby cationic vacancies for charge compensation.

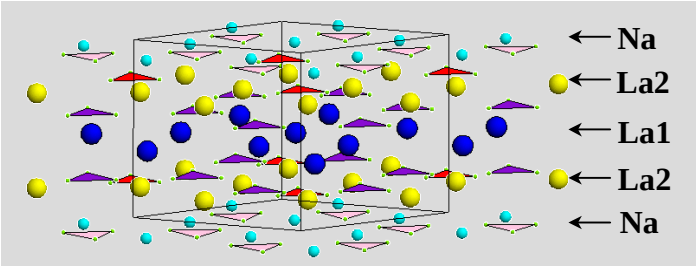

Fig. 4. View of the structure of the $Na_3La_9O_3(BO_3)_8$ crystal, showing the alternate layers of Na-$B(2)O(2)_3$ (z = 0), $B(1)O(1)_3$ (z = 0.21), La2 (z = 0.23), $B(3)O(3)_3$ (z = 0.32) and $La1O_4$ (z = 1/2, on the mirror plane), with BO_3 triangles aligned in rows along the *c* axis.

In conclusion, according to the above mentioned symmetry characteristics of the FLN spectra for Eu^{3+} located in the A, B, C, and D sites, the simulations of the corresponding energy level sequences performed for C_{4v}, C_2, C_{3v}, and C_{4v} crystal field potentials, respectively, yield ^7F_J schemes in very good agreement with the experimental data, as can be seen in Table 1.

Initially the spectrum for Eu^{3+} in site B was simulated by considering the C_{2v} potential, but the agreement between observed and calculated energy levels was found to improve by introducing the complex S_q^k parameters of symmetry C_2, which in turn agrees with the fact that the $La2O_9$ site, to which the Eu^{3+} B-spectrum corresponds, is a very distorted MSAP.

The C_{4v} characteristics of the Eu^{3+} spectrum in site A, the most abundant one, fully reflect the nature of the $La1O_8$ environment, with La1 located on the mirror plane in the *c*-axis. The crystal field parameters involved in the description of C_{4v} are the same as for D_{4h} and D_4 potentials, but the presence of the $^5D_0 \rightarrow {}^7F_0$ transition undoubtedly discards these latter symmetries.

Spectra for Eu^{3+}-A and D sites, both with C_{4v} symmetry characteristics, have been reproduced through very different sets of crystal field parameters (see Table 3), which lead to very different Eu^{3+} local environments.

On the other hand, the inferred existence of an extended NaO_{10} environment for Eu^{3+} in site C can be understood on the basis of the poor or incomplete effective shielding of Eu^{3+} by the six nearest coordinated oxygen atoms that form the distorted octahedral coordination in the crystallographic description of the structure. Thus, the crystal field generated by the ligands in the first coordination sphere is, in this case, not a good enough approximation for the crystal field perturbation felt by the Eu^{3+} doping cation, an effect which was previously described in other well known Eu^{3+}-doped borate layered crystal, $YAl_3(BO_3)_4$ [17].

#91301 - $15.00 USD Received 3 Jan 2008; revised 7 Feb 2008; accepted 10 Feb 2008; published 12 Feb 2008

6. Conclusion

By using the fluorescence line narrowing technique we have demonstrated the existence of four different local environments around the RE ions in $Na_3La_9O_3(BO_3)_8$ crystal. On the ground of the experimental results, the crystal-field analysis and simulation of the energy level schemes allow to connect the predicted symmetry of the resolved sites with the crystal structure. In conclusion, though RE ions may occupy the crystallographic sites for La1, La2, Na**,** and B3 the luminescence results suggest that the first possibility is the most likely to occur.

Acknowledgments

This work was supported by the Spanish Government MEC (MAT2004-03780) and the Basque Country Government (IT-331-07).

Appendix

Table 1. Summary of spectroscopic results and assignment of Eu^{3+} positions in $Na_3La_9O_3(BO_3)_8$ crystal

SITE	Characteristics of FLN Spectrum	Assignment of cationic site for Eu^{3+}
A	*Degeneracy for $^7F_1$ and $^7F_2$ levels*: 2 and 4 energy levels, respectively. *$^5D_0 \rightarrow {}^7F_0$ transition observed* Expected local symmetry: C_{4v} or C_4 Lifetime ($^5D_0$): 1.87 ms	La1 site, with crystallographic $La1O_8$ coordination: distorted square antiprism of C_{4v} symmetry
B	*Degeneracy for $^7F_1$ and $^7F_2$ levels*: Fully removed, 3 and 5 energy levels, respectively. *$^5D_0 \rightarrow {}^7F_0$ transition observed* Expected local symmetry: C_{2v} or lower C_2, C_s Lifetime ($^5D_0$): 1.73 ms	La2 site, with crystallographic $La2O_9$ coordination: distorted monocapped square antiprism of C_{2v} or lower symmetry
C	*Degeneracy for $^7F_1$ and $^7F_2$ levels*: 2 and 3 energy levels, respectively. *$^5D_0 \rightarrow {}^7F_0$ transition observed* Expected local symmetry: C_{3v} Lifetime ($^5D_0$): 1.32 ms	Na site, with an extended NaO_{10} environment (4 additional oxygens close to the NaO_6 crystallographic distorted octahedron) tetracapped trigonal prism with C_{3v} symmetry
D	*Degeneracy for $^7F_1$ and $^7F_2$ levels*: 2 and 4 energy levels, respectively. *$^5D_0 \rightarrow {}^7F_0$ transition observed* Expected local symmetry: C_{4v} or C_4	Suggested ordered arrangement of perturbed B3 sites, with an extended $B3O_9$ environment of oxygens up to~ 3.7 Å, with C_{4v} symmetry

#91301 - $15.00 USD Received 3 Jan 2008; revised 7 Feb 2008; accepted 10 Feb 2008; published 12 Feb 2008

Table 2. Observed and calculated energy levels (cm^{-1}) of Eu^{3+} optical centers observed in $Na_3La_9O_3(BO_3)_8$ crystal

	SITE A		**SITE B**		**SITE C**		**SITE D**	
λ_{EXC} (nm)	581.9		581.7		580.4		580.0	
SYMMETRY	**C_{4v}**		**C_2**		**C_{3v}**		**C_{4v}**	
$^{2S+1}L_J$	E_o	E_c	E_o	E_c	E_o	E_c	E_o	E_c
^7F_o	0	0	0	0	0	0	0	0
$^7F_1$	245	239	273	286	217	213	197	188
	316	325	350	342	286	294	266	284
			446	441				
$^7F_2$	904	898	904	891	1124	1123	710	702
	975	966	922	914	1194	1196	748	759
	1358	1367	1036	1041	1374	1374	797	820
	1372	1382	1059	1070			1050	1030
			1188	1195				
$^7F_3$	1840	1834	1822	1838	1862	1878		2022
	1950	1939	1838	1840	-	1970	2074	2080
	1981	1970	1863	1871	2032	2025	-	2087
	2034	2063	1898	1897	-	2061	-	2146
	2228	2196	1945	1932	2081	2079	2158	2152
			1973	1973				
			2021	2010				
$^7F_4$	-	2356	2586	2584	-	2680	2449	2450
	-	2660	2597	2606	2799	2795	2564	2556
	2852	2845	2848	2839	2853	2856	2641	2635
	2966	2965	2864	2867	2954	2955	-	2688
	-	2996	2936	2946	3035	3041	2742	2741
	-	3007	2968	2966	-	3223	2820	2824
		3157	2984	2991			-	2907
			-	2996				
			3104	3089				
$^7F_5$	-	3519	3732	3726	-	3580	-	3191
	-	3609	3739	3734	-	3643	3242.6	3244
	3728	3732	3852	3854	3780	3780	-	3356
	3741	3744	3875	3876	3875	3875	3379	3375
	-	3823	-	3941	3889	3886	3438	3442
	-	3898	-	3946	3999	4002		3460
	-	4017	4002	4012	-	4122	3496	3494
		4041	-	4017			-	3568
			4104	4102				
			-	4157				
			-	4179				
$^7F_6$	4747	4763	-	4728	-	4337		
	-	4791	4736	4730	-	4348		
	4813	4806	-	4878	-	4362		
	-	4950	-	4883	-	4374		
	4991	4987	4936	4947	4648	4661		
	-	5081	-	4962		4684		
	-	5091	-	5010	-	4728		
	-	5095	5031	5030	-	4768		
	-	5199	-	5071	4782	4771		
		5202	-	5113				
			-	5115				
			-	5120				
			5130	5126				

#91301 - $15.00 USD Received 3 Jan 2008; revised 7 Feb 2008; accepted 10 Feb 2008; published 12 Feb 2008

Table 3. Phenomenological crystal-field parameters (cm^{-1}) for Eu^{3+} optical centers observed in $Na_3La_9O_3(BO_3)_8$

	SITE A		**SITE B**		**SITE C**		**SITE D**
λ_{EXC} (nm)	581.9		581.7		580.4		580.0
Symmetry	C_{4v}		C_2		C_{3v}		C_{4v}
B_0^2	371(24)	B_0^2	426(19)	B_0^2	312(18)	B_0^2	357(27)
B_0^4	-1415(45)	B_2^2	113(15)	B_0^4	205(31)	B_0^4	-1694(35)
B_4^4	-1455(29)	B_0^4	1166(35)	B_3^4	1307(16)	B_4^4	102(29)
B_0^6	1581(75)	B_2^4	665(24)	B_0^6	-60(32)	B_0^6	-721(47)
B_4^6	-785(46)	S_2^4	-38(58)	B_3^6	-1520(23)	B_4^6	674(27)
		B_4^4	-282(37)	B_6^6	-822(23)		
		S_4^4	202(45)				
		B_0^6	-1(40)				
		B_2^6	48(33)				
		S_2^6	-177(48)				
		B_4^6	199(45)				
		S_4^6	-125(70)				
		B_6^6	935(31)				
		S_6^6	-690(58)				
L_{obs}/L [a]	19/37	L_{obs}/L	34/49	L_{obs}/L	19/33	L_{obs}/L	18/37
σ [b]	14.8	σ	10.3	σ	6.6	σ	10.7

[a] L_{obs} is the number of observed Stark energy levels, and L the total number of energy levels in the indicated symmetry.

[b] $\sigma = \left[\sum (\Delta_i)^2 / (L_{obs} - p)\right]^{1/2}$, $\Delta = E_{obs} - E_{cal}$, p is the number of parameters.

#91301 - $15.00 USD Received 3 Jan 2008; revised 7 Feb 2008; accepted 10 Feb 2008; published 12 Feb 2008